Applied Geochemistry 87 (2017) 71–83

Contents lists available at ScienceDirect

Applied Geochemistry

journal homepage: www.elsevier.com/locate/apgeochem

Molybdenum (Mo) stable isotopic variations as indicators of Mo attenuation in mine waste-rock drainage

E.K. Skierszkan[a,*], J.S. Stockwell[b], J.W. Dockrey[b], D. Weis[c], R.D. Beckie[a], K.U. Mayer[a]

[a] Department of Earth, Ocean and Atmospheric Sciences, University of British Columbia, 2020-2207 Main Mall, Vancouver V6T 1Z4, Canada
[b] Lorax Environmental Services Ltd., 2289 Burrard St, Vancouver V6J 3H9, Canada
[c] Pacific Centre for Isotopic and Geochemical Research, Department of Earth, Ocean and Atmospheric Sciences, University of British Columbia, 2020-2207 Main Mall, Vancouver V6T 1Z4, Canada

ARTICLE INFO

Keywords:
Molybdenum isotopes
Adsorption
Mine waste-rock drainage
Weathering
Molybdenite
MC-ICP-MS

ABSTRACT

Measurements of molybdenum (Mo) stable isotopes (δ^{98}Mo) were applied along with conventional geochemical analyses of water and rock samples at a Mo mine in the USA to assess controls on Mo mobility in two unsaturated waste-rock storage facilities (WRSFs) that are differentiated by acidic and alkaline drainages. Unweathered waste rock, Mo ore, and mine tailings from the site were also analyzed to constrain the isotopic composition of the source of Mo entering mine drainage via weathering processes. The surfaces of weathered waste-rock samples were sequentially leached using a two-step chemical extraction to determine the distribution and isotopic composition of Mo among primary and secondary mineral assemblages.

The observed variation in δ^{98}Mo among all samples exceeded 5‰. The δ^{98}Mo of Mo-rich (> 340 µg/L) mine process water and pit wall runoff ranged from 0.6 to 0.7‰, which was equal within error to the average δ^{98}Mo of waste rock, tailings, and ore samples and indicated negligible isotopic fractionation during molybdenite oxidative dissolution. In contrast, drainage from the base of both waste-rock storage facilities was isotopically heavier, ranging from 1.6 to 1.9‰. Coupled δ^{98}Mo and Mo/SO_4^{2-} ratios in mine drainage and sequential chemical extractions of weathered waste-rock surfaces indicated that Mo adsorption onto mineral surfaces was most likely driving the increase in δ^{98}Mo in drainage from both WRSFs. Molybdenum stable isotope data provided a powerful tracer of processes controlling Mo mobility when used in conjunction with conventional geochemical analyses.

1. Introduction

Metal leaching from sulfide mineral oxidation in mining waste rock constitutes a global environmental challenge whose mitigation requires a detailed understanding of the mobility of metals within mine waste-rock storage facilities (WRSFs). Molybdenum is a transition metal that can reach elevated concentrations in water as a result of the weathering of sulfidic mine wastes (Goumih et al., 2013; Kaback and Runnells, 1980), in particular under alkaline conditions (Conlan et al., 2012). At elevated concentrations, excess Mo can be harmful, especially for ruminants, which are susceptible to molybdenosis (Barceloux, 1999). The World Health Organization recommends that Mo concentrations in drinking water should not exceed 70 µg/L (World Health Organization, 2011). Knowledge of the fate of this element within mine wastes is therefore necessary for their proper environmental management. However, the complexity of processes such as Mo release, adsorption, and precipitation, which may be simultaneously occurring in waste-rock environments, creates uncertainty regarding its fate. Long-term changes in pH and redox conditions in WRSFs further enhance the need to identify the processes of Mo attenuation and to anticipate changes in water quality in the decades following disposal.

The dominant Mo source in Mo-rich waste rock is the ore mineral molybdenite (MoS_2). Oxidative dissolution of molybdenite leads to the release of aqueous Mo in the form of the molybdate (MoO_4^{2-}) oxyanion (Smedley and Kinniburgh, 2017). Other sulfide minerals (*e.g.*, pyrite) have Mo concentrations that are orders of magnitude lower (Greaney et al., 2016; Pichler and Mozaffari, 2015), and the main minerals that host Mo in silicate rocks are Ti-bearing minerals, such as titanite and ilmenite, which are highly resistant to chemical weathering in comparison with sulfides (Chappaz et al., 2014; Greaney et al., 2016; Smedley and Kinniburgh, 2017).

In oxidized circumneutral to alkaline aqueous environments, molybdate dominates the aqueous Mo pool. Molybdate is strongly adsorbed onto mineral surfaces under acidic conditions, with maximal

* Corresponding author.
E-mail address: eskiersz@eos.ubc.ca (E.K. Skierszkan).

http://dx.doi.org/10.1016/j.apgeochem.2017.10.008
Received 11 April 2017; Received in revised form 13 October 2017; Accepted 16 October 2017
Available online 21 October 2017
0883-2927/

adsorption in the range of pH 4 to 5 (Goldberg et al., 1996; Gustafsson, 2003; Xu et al., 2006). Molybdate adsorption is weaker under alkaline conditions, becoming minimal at pH > 8 (Goldberg et al., 1996). In alkaline mine drainage, an alternative molybdate sink is the precipitation of secondary minerals such as powellite ($CaMoO_4$), wulfenite ($PbMoO_4$), and $NiMoO_4$ (Conlan et al., 2012; Essilfie-Dughan et al., 2011).

Recent studies have shown that Mo stable isotope analyses can serve as a complementary tool to track the environmental fate of molybdenum (Siebert et al., 2015). Current knowledge of Mo isotopic fractionation was reviewed by Kendall et al. (2017). A survey of Mo isotope compositions in rivers around the world revealed that a creek receiving drainage from a major Mo mine (Clear Creek, Colorado, USA) constituted an end-member with the highest Mo concentration (49 μg/L) and lightest Mo isotopic composition (Archer and Vance, 2008). Recent field waste-rock weathering experiments have also shown that mine drainage becomes enriched in heavier Mo isotopes relative to source minerals as a result of Mo attenuation processes (Skierszkan et al., 2016). Field-based studies examining Mo stable isotope systematics during weathering and transport in rivers and soils demonstrate preferential removal of light Mo isotopes, leading to isotopically heavier fluids (King et al., 2016; Pearce et al., 2010; Siebert et al., 2015; Skierszkan et al., 2016; Wang et al., 2015). The known isotopic fractionation factors for Mo attenuation reactions all indicate preferential removal of light isotopes from aqueous solutions, leading to a heavier isotopic signature of dissolved Mo. In oxidized aqueous environments, this result has been shown for adsorption onto Fe- and Mn-(oxy)hydroxides (Barling and Anbar, 2004; Goldberg et al., 2009; Wasylenki et al., 2008). In anoxic and sulfidic environments, molybdate can be converted to thiomolybdate ($MoO_xS_{4-x}^{2-}$), which preferentially accumulates light Mo isotopes and readily precipitates from solution (Nägler et al., 2011; Tossell, 2005). The evolution of the Mo isotopic composition in solution is therefore controlled by the extent of Mo attenuation via one or more of the aforementioned Mo removal pathways. As a result, Mo isotopic fractionation can be a useful indicator of Mo attenuation in WRSFs.

In this work, the primary objective was to determine the process of Mo attenuation within two large (> 130 million tons) WRSFs using Mo stable isotopes along with conventional geochemical analyses in mine drainage samples. Molybdenum stable isotopes were also analyzed in waste rock, tailings, and ore samples to constrain the isotopic composition of the source of Mo at the study site. In addition, the surfaces of visibly weathered waste-rock samples were subjected to sequential chemical extractions to determine whether Mo was being retained and isotopically fractionated on mineral surfaces during reactive transport. Finally, surface water and groundwater samples from the mine site were analyzed to determine whether mine drainage Mo was isotopically distinguishable from natural water. The results obtained here provide an overview of the extent of Mo stable isotope variations that may be encountered in rocks, mine drainage and natural waters at the catchment scale and relate these variations to processes controlling Mo during weathering and transport.

2. Study site

2.1. Local climate and geology

Samples were collected at the Thompson Creek Molybdenum Mine, located in the Central Rocky Mountains in Idaho, USA (Fig. 1). Precipitation falls mostly as winter snow, with occasional summer thunderstorms. Snowmelt represents > 70% of runoff, and freshet (peak flow) typically occurs in April or May (Dockrey and Stockwell, 2012). Molybdenite (MoS_2) was emplaced by a Late Cretaceous magmatic intrusion into shales and carbonaceous argillites (Dockrey and Stockwell, 2012). This entire sequence was covered much later by Eocene volcanic rock. Molybdenite is mainly concentrated within the intrusion and extends slightly into the metasedimentary country rock. Volcanic, metasedimentary and intrusive waste rocks have been stockpiled in two WRSFs occupying different valleys adjacent to the open pit for close to three decades of mining. During operations, waste was classified as *potentially acid generating* (PAG) or *non-acid generating* (NAG) based on its carbonate and sulfur content. The *Buckskin WRSF* served as the primary repository for *NAG* material, and the *Pat Hughes WRSF* mainly comprised *PAG* material (Fig. 1). PAG waste emplaced in the Buckskin WRSF is encapsulated within a layer of NAG waste. Consequently, drainage from the Buckskin WRSF has remained alkaline, with a pH of approximately 8, over the course of the mine life despite ongoing sulfide oxidation (Dockrey and Stockwell, 2012). Molybdenum concentrations have also risen steadily since 2008, ranging between approximately 60 and 80 μg/L. Drainage from the PAG-rich Pat Hughes WRSF was historically alkaline and had Mo concentrations ranging from tens to hundreds of μg/L. However, in 2006, drainage became acidic and since then has remained persistently at a pH of approximately 4.5 with Mo concentrations < 10 μg/L (Dockrey and Stockwell, 2012).

2.2. Site hydrology

Both WRSFs occupy distinct catchments (Fig. 1). Water movement generally follows regional topography; in valley bottoms, fast-flowing shallow colluvial/alluvial aquifers historically drained into Thompson Creek. Shallow bedrock, either volcanic or metasedimentary, is also recharged from the overlying colluvium/alluvium. Deeper bedrock aquifers have slower and upward groundwater flow driven by recharge in the neighboring mountains (Lorax Environmental Services Ltd., 2011a). The flow of shallow groundwater and flow within WRSFs respond strongly to seasonal variations, in particular, melting of the winter snowpack during freshet. During baseflow (October-December), there is an increase in the proportion of groundwater discharge that contributes to flow at the mine drainage sampling stations (Lorax Environmental Services Ltd., 2011a). In the fall of 2014, shortly after the first sampling round in this study, cutoff walls were installed within the shallow colluvial/alluvial aquifers downgradient of both WRSFs to prevent leakage of mine drainage.

3. Sample collection and preparation

3.1. Water sampling and storage

Water was sampled during the 2014 and 2015 fall baseflows and in spring 2016 during freshet. Groundwater and surface water samples included both locations that were impacted and those that were unimpacted by mine drainage. Mine drainage samples were collected from discharge points directly at the base of WRSFs. In addition, mine process water collected within the tailings pond and runoff percolating within the open pit of the mine were analyzed to determine the Mo isotopic signature of aqueous Mo directly after oxidative dissolution of MoS_2. A brief description of the water sampling locations is provided in Table 1, and sampling locations are shown in Fig. 1.

During water-sample collection, temperature, electrical conductivity, oxidation-reduction potential, pH, and dissolved oxygen were measured with a flow-through cell connected to an MP-20 multi-probe instrument (QED Environmental Systems, Ann Arbor, Michigan, USA) that was calibrated daily using pH 4 and pH 7 buffers. Electrical conductivity, oxidation-reduction potential and dissolved oxygen measurements were considered to be qualitatively accurate. Shallow groundwater and surface water were collected using a peristaltic pump and dedicated HDPE tubing and filtered in-line using 0.45-μm Geotech dispos-a-filters™. Deeper groundwater samples were drawn using either Hydrolift-2 Actuators connected to dedicated Waterra Inertial Lift Pumps or bladder pumps connected to dedicated tubing in each well. Prior to sampling, groundwater was purged, and field chemistry

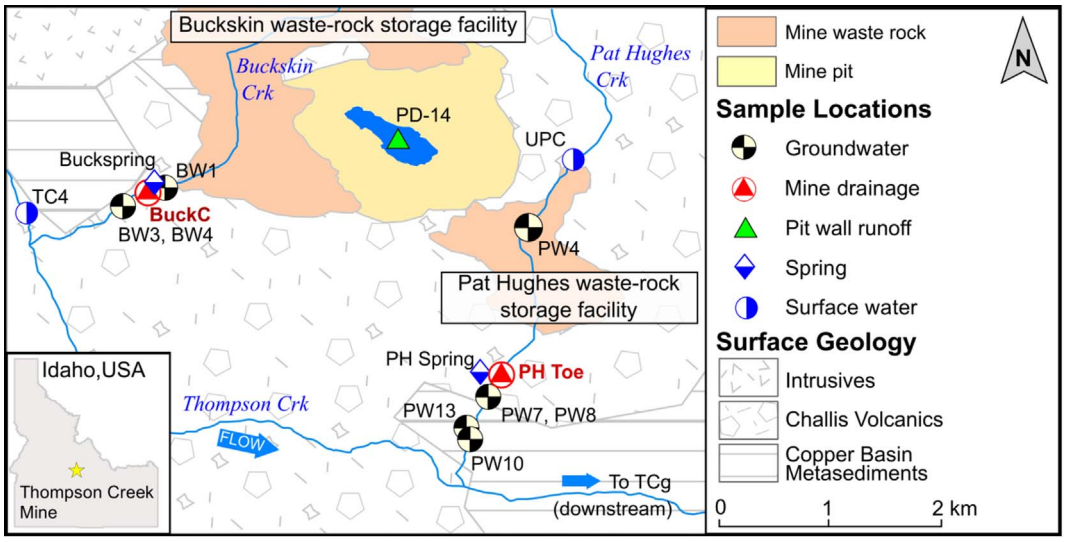

Fig. 1. Site location map showing sampling locations, waste-rock storage facilities, open pit and surficial geology. Three sampling locations (TCg, BC3A and Sunbeam) fall outside of the extent of this map. Samples are described in Table 1. Surface geology is taken from the USGS (2005).

parameters and drawdown were monitored at regular intervals to ensure that representative formation water was being collected. Samples were filtered in-line and drawn after stabilization of field parameters.

All water samples were stored in coolers with icepacks until refrigeration in the laboratory. Samples for sulfide analysis were preserved using NaOH and Zn-acetate. Alkalinity titrations were conducted using the Gran Method on the same day as sample collection. Water samples for metals and Mo isotopic analysis were collected into acid-washed HDPE bottles and preserved with sub-boiled HNO_3 to pH < 2. Metal blanks were monitored during each sampling round by passing ultrapure > 18.2 mΩ water though the peristaltic pump apparatus, including the tubing and filter, and preserved with HNO_3 in the same manner as the samples; Mo concentrations measured in the blanks ranged from 0.002 to 0.09 μg/L. Sample Mo concentrations ranged from 0.29 to 3260 μg/L; in the majority of samples, the blank would have contributed less than 5% of the Mo, although it is possible in five (out of thirty) samples with Mo concentrations less than 2 μg/L that the blank contribution could have been greater.

3.2. Rock sampling and preparation

Waste-rock and ore samples representing the major lithologies present at the site were obtained from the mine's geology department collection or directly from WRSFs. To eliminate the effects of chemical weathering on samples collected in the field, their outer faces were removed using a rock saw. Rocks were pulverized using a ring-mill, and aliquots were weighed into Savillex® PFA vials for hotplate dissolution using the method of Connelly et al. (2006). A sample of a white precipitate forming in basal drainage at the Pat Hughes WRSF was also collected and frozen in the field with dry ice. It was thawed in the laboratory, and water contained in the sample was removed by centrifugation. The precipitate was then dissolved in a MARS6 OneTouch Microwave Digestion System (CEM Corporation, Matthews, North Carolina, USA) using HCl-HF-HNO_3 that was a 5× scale-up of the protocol of Axelsson et al. (2002).

All acids used for sample digestions were purified in-house from concentrated reagent-grade acids by sub-boiling distillation, and

Table 1
Description of water sampling locations.

Sample	Type	Description
Pat Hughes Catchment		
PW10	Groundwater	Deep groundwater from metasedimentary bedrock aquifer
PW13	Groundwater	Deep groundwater from metasedimentary bedrock aquifer
PW4	Groundwater	Groundwater/mine drainage mixture from a well drilled into the base of the Pat Hughes WRSF
PW7	Groundwater	Intermediate groundwater from metasedimentary bedrock aquifer
PW8	Groundwater	Shallow groundwater from collivial/alluvial aquifer downgradient of the Pat Hughes WRSF
UPC	Creek	Upper reach of Pat Hughes Creek, upstream of mining activities
PH Toe	Mine drainage	Mine drainage outflowing from the base of the Pat Hughes WRSF
PH Spring	Spring	Spring draining into Pat Hughes Creek. The upper reach of the drainage contains a small amount of Pat Hughes waste rock
Buckskin Catchment		
BW1	Groundwater	Deep artesian groundwater from metasedimentary bedrock aquifer
BW3	Groundwater	Deep artesian groundwater from metasedimentary bedrock aquifer
BW4	Groundwater	Shallow groundwater from collivial/alluvial aquifer below bottom of Buckskin WRSF
BuckC	Mine drainage	Mine drainage outflowing from the base of the Buckskin WRSF
BuckSpring	Spring	Spring draining into Buckskin Creek below the base of the Buckskin WRSF
Tailings Pond and Open Pit Drainag		
PD-14	Pit wall runoff	Runoff from the mine's open pit
TP-14	Process water	Mine process water
Other Catchments		
Sunbeam HS	Groundwater	Hot spring (77 °C) surfacing ~15 km W of mine site
TC4	Creek	Thompson Creek, upstream of mining activities and upstream of the confluence with Buckskin Creek
TCg	Creek	Thompson Creek, downstream of mining activities and of the confluence with Pat Hughes and Buckskin Creeks
BC3A	Groundwater	Deep groundwater from metasedimentary bedrock aquifer, in Bruno Creek Drainage, 3 km E of Pat Hughes WRSF

Table 2
Molybdenum abundance and isotopic composition in waste rock, ore, and tailings.

	Lithology	Mo µg/g	δ^{98}Mo[a] ‰	± 2 SD[b]	n[c]
Molybdenite Ores					
IHG1	intrusive	1,320	0.39	0.01	3
IHG2	intrusive	4,820	0.09	0.03	3
IHG3	intrusive	1,570	−0.02	0.09	3
MSO1	metasedimentary	1,270	−0.07	0.06	3
MSO2	metasedimentary	218	1.10	0.06	3
Mine Tailings					
TAILS	tailings	27	0.14	0.06	3
FT-15	tailings	55.5	0.20	–	1
FT-16	tailings	71.5	0.09	–	1
TC-16	tailings	59.4	0.07	–	1
DFT-16	tailings	135[d]	0.25	–	1
Waste Rock					
BS-QTZW-15-2	intrusive-hosted qtz-MoS_2-FeS_2	240[d]	*0.98*	*0.06*	2
PHIW15-1	intrusive	3,300	0.71	–	1
PHIW15-4	intrusive	289	1.29	–	1
PHIW16-3	intrusive	7,400[d]	*0.95*	*0.03*	2
PHIW16-5	intrusive	380	−0.10	–	1
PHIW16-1 GM	intrusive (feldspar matrix)	2.21	1.28	–	1
PHIW16-1 Py	massive pyrite	0.165			
IW1	intrusive	3.8	−0.88	0.08	3
IW2	intrusive	0.40			
IW3	intrusive	60.1	0.83	0.02	3
IW1 w/Mo	intrusive	175	1.24	0.08	3
IW3 w/Mo	intrusive	175	0.17	0.08	3
MSW2	metasedimentary	9.08	0.65	0.06	3
MSW3	metasedimentary	81	0.84	0.08	3
IW4	metasedimentary	52	1.22	0.07	2
MSW1 w/Mo	metasedimentary	533	1.16	0.01	3
BS-MSW-15-1	metasedimentary	0.39			
BS-MSW-15-2	metasedimentary	0.83			
BS-MSW-15-6	metasedimentary	10.0	0.94	–	1
BS-MSW-15-7	metasedimentary	1.40			
BS-MSW-15-9	metasedimentary	28.9	0.43	–	1
PH-MSW-16-1	metasedimentary		0.11	–	1
VW1	volcanic	0.66	0.3	0.1	3
VW2	volcanic	0.99	0.28	0.04	3
VW3	volcanic	0.28			

The highest significant digit in the 2 SD of each measurement was used to define the number of significant digits shown in Table 2.

[a] δ^{98}Mo expressed relative to NIST-SRM-3134 = +0.25‰.

[b] 2 SD for triplicate or duplicate analysis of a single sample solution on the MC-ICP-MS. Dashed lines indicates the samples that were only analyzed once, in which case the 2 standard error was < 0.04‰ for 30 measurement cycles on the MC-ICP-MS. Italics indicate δ^{98}Mo measurement and 2 SD for a full duplicate (including rock digestion and ion-exchange chemistry).

[c] Number of replicate analyses on the MC-ICP-MS.

[d] Average of duplicate analysis on ICP-MS.

dissolutions were performed in metal-free Class 1000 clean laboratories at the Pacific Centre for Isotopic and Geochemical Research (PCIGR) at the University of British Columbia (Vancouver, Canada).

3.3. Characterization of weathered waste-rock surfaces

The Mo distribution and isotopic composition on the surfaces of weathered waste rock were characterized by sequential chemical extractions and X-ray diffraction. The chemical extraction protocol was modified from Wiederhold et al. (2007) but downscaled proportionally due to the small amounts of surface coatings that were recovered from each sample. Sequential chemical extractions are operationally defined: in this case, they were designed to extract the Mo mobilized under reducing conditions in "*Step 1*" using 1 M $NH_2OH{\cdot}HCl$-1 M HCl and under oxidizing conditions in "*Step 2*" using *aqua regia*. Step 1 grouped amorphous and crystalline Fe-(oxy)hydroxide minerals as well as water-soluble and exchangeable phases; we did not attempt to distinguish Mo association among these reservoirs. Step 2 targeted oxidizable sulfide minerals.

The weathered waste-rock samples selected for extractions were coated in orange Fe-(oxy)hydroxides. Surface minerals were scraped using silicon-carbide sandpaper and homogenized using a mortar and pestle. Qualitative mineralogy was obtained by X-ray diffraction (XRD) using a Siemens Bruker D5000 Bragg-Brentano diffractometer over a 3-80° 2θ range with a CoKα radiation source. Silicate and sulfide grains, which are insoluble in NH_2OH-HCl/HCl, were inevitably entrained into the sample during scraping (Dragovich, 2006). As a result, the elemental abundances obtained in Step 1 constitute lower limits for surface coatings in weathered waste rock.

For Step 1, 2 mL of 1 M $NH_2OH{\cdot}HCl$/ 1 M HCl solution was added to 100-mg sample aliquots. These mixtures were then placed in a 90 °C water bath contained in a horizontal shaker for 4 h and vortexed every 30 min. The mixtures were then centrifuged at 3000 rpm for 15 min, and the resulting supernatants were collected and filtered (0.2 µm). To maximize recoveries, the remaining residues were subjected to the same procedure for 2 h, and the supernatant was once again centrifuged, filtered and added to the initial supernatant. The extracted solutions were preserved in 2% HNO_3 for analysis of elemental concentrations by inductively-coupled plasma optical-emission spectroscopy (ICP-OES).

The solid residues remaining after Step 1 were dried overnight at 75 °C, after which, in Step 2, they were weighed into PFA vials and digested in 3 mL of *aqua regia* (a 3:1 concentrated HCl-HNO_3 mixture) on a hotplate for 24 h at 150 °C. The digestate was extracted after centrifugation for 15 min at 3000 rpm, and to maximize recoveries, the remaining solids were rinsed and centrifuged three times in 1.5 mL of > 18.2 mΩ H_2O, with the additional supernatant added to the initial *aqua regia* solution. This recovered solution was dried down, treated three times with a 200-µL drop of concentrated HNO_3, and re-dissolved in a 2% HNO_3 solution for analysis by ICP-OES. The reagent blank for the chemical extraction represented at most 0.4% of the Mo content in the samples. One sample was processed in duplicate, and the relative percent differences of Mo content between duplicates were 4% for Step 1 and 13% for Step 2. The Mo isotope analysis of Step 1 duplicates was reproduced within 0.01‰.

3.4. Analytical methods

Anions and sulfide in water samples were analyzed within 1 week of sampling using ion chromatography and colorimetric methods, respectively, at ALS Environmental (Burnaby, Canada). Abundances of Al, Ca, Mo, S, Fe, K, Mg, Mn, Na, Si, and Zn were determined in sequential chemical extraction samples by ICP-OES (Varian 725-ES) with an external calibration standard and europium as an internal-drift correction standard. For water samples, major element concentrations were also determined by ICP-OES. The accuracy of the ICP-OES was monitored by analysis of a secondary ICP calibration standard solution: Analyses were on average accurate within 4% relative to expected values for the secondary standard (Supplementary Table S1). ICP-OES external reproducibility was assessed by the relative standard deviation (RSD) of replicate analyses of standard solutions and was typically better than 3% and no worse than 6% (Supplementary Table S2). Absolute charge balance errors for water sample analyses were on average 3% and always better than 10% (Table 3).

Trace element contents in rock and water samples were determined by inductively-coupled plasma mass spectrometry (ICP-MS, Agilent 7700×). The instrument was calibrated with a multi-element standard solution, and indium was used for internal drift correction. The external reproducibility of trace metal ICP-MS analyses was on average 4%, as determined by calculation of the relative standard deviation of replicate analyses of standards (Supplementary Table S3). ICP-MS accuracy was verified with analyses of Mo and Pb contents in the USGS BCR-2 reference material; these were equal within error to the certified values

Table 3A
Water-sample chemistry: Field parameters and anions concentrations.

Sample	Type	Date	Field parameters				Anions				
			Alkalinity mg/L as $CaCO_3$	pH	Cond. mS/cm	C.B.E.[a] %	Cl^- mg/L	F^- mg/L	NO_3^- mg/L as N	SO_4^{-2} mg/L	S^{2-} mg/L
Pat Hughes Catchment											
PW10	GW	Oct-15	231	7.25	0.67	1.0	2.1	0.7	< dl	156	0.061
PW13	GW	Apr-16	287	7.14	0.85	−0.9	< dl	0.6	< dl	180	0.099
PW4	GW	Oct-15	27	5.62	0.53	0.8	21	0.3	1.9	212	–
PW4	GW	Apr-16	3	4.83	1.33	−9.9	36	2.1	2.4	638	–
PW7	GW	Oct-15	208	7.37	0.70	3.5	12	0.3	0.8	179	–
PW7	GW	Apr-16	207	7.28	0.79	−4.1	9.2	0.3	0.9	196	–
PW8	GW	Oct-15	118	6.60	0.66	6.2	3.7	0.13	3.1	238	–
PW8	GW	Apr-16	70	7.10	0.50	−0.8	2.2	0.13	3.7	144	–
UPC	Creek	Apr-16	36	6.25	0.09	2.3	0.72	0.047	0.01	3.6	–
PH Spring	GW spring	Apr-16	52	7.71	0.44	3.3	1.1	0.049	4.0	128	–
PH Toe	WRSF drainage	Oct-14	11	4.54	1.77	7.9	23	2.7	12	1,170	–
PH Toe	WRSF drainage	Oct-15	11	4.86	2.02	1.5	19	3.6	12	1,290	–
PH Toe	WRSF drainage	Apr-16	18	4.42	3.56	−4.8	23	9.0	11	2,410	–
Buckskin Catchment											
BW1	GW	Apr-16	81	7.93	0.31	−2.1	1.2	0.27	< dl	59.1	0.0032
BW3	GW	Oct-14	128	7.33	0.28	−5.8	1.8	0.21	< dl	41.7	–
BW3	GW	Oct-15	116	7.94	0.30	4.4	1.8	0.20	< dl	41.4	–
BW4	GW	Oct-15	130	7.16	1.75	2.8	< dl	< dl	4.5	921	–
BW4	GW	Apr-16	135	7.18	0.71	−1.4	< dl	0.21	0.9	205	–
BuckC	WRSF drainage	Oct-14	152	7.75	2.19	3.3	< dl	< dl	14	1,260	–
BuckC	WRSF drainage	Oct-15	149	7.95	2.30	2.3	< dl	< dl	12	1,270	–
BuckC	WRSF drainage	Apr-16	135	7.58	2.36	1.4	< dl	< dl	9.1	1,120	–
BuckSpring	GW spring	Apr-16	126	7.80	0.27	1.9	0.65	0.14	0.009	7.5	–
Process Water and Pit Wall Runoff											
PD-14	Pit Wall Runoff	Oct-14	56	8.81	0.70	−2.9	3.3	1.6	0.2	243	–
TP-14	Process Water	Oct-14	47	7.53	3.86	3.0	341	0.53	1.2	1,830	–
Other Nearby Catchments											
TC4	Creek	Oct-14	53	6.70	0.10	−4.9	< dl	0.08	< dl	10	–
TC4	Creek	Oct-15	47	6.44	0.11	2.0	< dl	0.07	< dl	11	–
TCg	Creek	Oct-14	81	7.38	0.20	−2.9	1.0	0.13	< dl	31	–
TCg	Creek	Oct-15	114	6.79	0.21	−7.4	0.82	0.11	< dl	30	–
Sunbeam	Hydrothermal GW	Apr-16	121	9.40	0.43	−5.8	11	16	< dl	42	5.9
BC3A	GW	Oct-15	218	7.24	0.48	1.8	1.8	0.35	< dl	52	–

WRSF = waste-rock storage facility; GW = groundwater.
– Indicates that the parameter was not analyzed; < dl indicates below detection limit.
The highest significant digit in the 2 SD of each measurement was used to define the number of significant digits shown in Table 3.
[a] C.B.E. = charge balance error, calculated using PHREEQC.

(Schudel et al., 2015; Wilson, 1997; Supplementary Table S4). The reproducibilities for water, rock, and sequential chemical extraction samples were verified by analysis of full sample duplicates by ion chromatography, ICP-OES, and ICP-MS (Supplementary Table S5).

The geochemical code PHREEQC (Parkhurst and Appelo, 2013) was used to calculate mineral saturation indices in water samples using the wateq4f database, to which powellite and wulfenite solubility constants were added as described in Conlan et al. (2012) and Skierszkan et al. (2016).

Aliquots for Mo isotope analyses were weighed into Savillex® PFA beakers and a ^{97}Mo-^{100}Mo double spike was added to correct for laboratory and instrumental mass fractionation. Samples were purified using ion-exchange chemistry as described in Skierszkan et al. (2015, 2016). Column blanks contained on average 2.5 ng of Mo and always less than 5 ng. Whenever possible, > 500 ng of sample Mo was loaded onto columns to minimize the contribution from the blank. Molybdenum isotope ratios were determined using a Nu Plasma MC-ICP-MS (Nu 21, Nu Instruments Ltd., Wrexham, UK) connected to a DSN-100 desolvating nebulizer for sample introduction. For each batch of samples, accuracy was monitored by analyzing a reference material (*e.g.*, BCR-2, SDO-1 or seawater) along with samples through the full ion-exchange and analytical procedure. Molybdenum isotope compositions are reported using the $\delta^{98}Mo$ notation:

$$\delta^{98}Mo_{sample}(‰) = \left(\frac{\left(\frac{^{98}Mo}{^{95}Mo}\right)_{sample}}{\left(\frac{^{98}Mo}{^{95}Mo}\right)_{standard}} - 1 \right) \times 1000 \quad (1)$$

Molybdenum isotope data presented in this study follow the convention recommended by Nägler et al. (2014), whereby $\delta^{98}Mo$ values are normalized to NIST-SRM-3134 = + 0.25‰. The long-term average 2 SD reproducibility for analyses of the in-house Mo isotope standard "Mo(UBC)" in our laboratory is 0.07‰ (n = 244). For the Mo stable isotope analysis of samples reported in this study, 33% of the samples were analyzed in triplicate on the MC-ICP-MS, and the average 2 SD uncertainty for all sample replicate analyses was 0.06‰ (n = 31). 5% of the samples were analyzed as full duplicates (including digestion and ion-exchange chemistry as applicable), with a 2 SD reproducibility better than 0.06‰.

4. Results

4.1. Source characterization: rocks

Volcanic waste rock and pyrite were negligible sources of Mo for mine drainage. Volcanic waste rock, emplaced well after the ore-building intrusion, was characterized by Mo contents < 1 μg/g and $\delta^{98}Mo$ values of 0.3–0.4‰ (Table 2). These values are similar to the Earth's upper crustal Mo abundance of approximately 1 μg/g (Rudnick

Table 3B
Water-sample chemistry: Metals and metalloids concentrations and Mo isotope ratios.

Sample	Date	Metals and metalloids										δ^{98}Mo[a] ‰	± 2 SD or 2 SE[b]	n	Mineral Saturation	
		Ca mg/L	K mg/L	Mg mg/L	Na mg/L	Si mg/L	Al µg/L	Fe µg/L	Mn µg/L	Mo µg/L	Pb µg/L				powellite	wulfenite
Pat Hughes Catchment																
PW10	Oct-15	83	3.1	44.6	4.49	1.3	1	1,120	21	0.1	0.009	2.91	*0.07*	1	−3.1	N/A[c]
PW13	Apr-16	70.4	4.0	64.1	7.97	4.71	1.2	783	61.1	0.29	< dl	4.8	0.1	2	−4.0	N/A[c]
PW4	Oct-15	53	1.2	13.59	42.4	1.6	180	< dl	190	7	0.05	2.13	*0.04*	1	−2.7	−1.7
PW4	Apr-16	99.9	1.4	37.2	58.3	5.8	7,100	361	10,450	32.2	0.793	1.19	*0.03*	1	−2.0	−0.1
PW7	Oct-15	92.8	2.0	38.7	22.7	4.5	< dl	< dl	< dl	3.3	0.006	1.55	*0.04*	1	−2.9	−3.8
PW7	Apr-16	81.8	1.81	33.9	20.0	5.6	75	15.8	0.14	4.48	< dl	1.59	*0.03*	1	−2.8	N/A[c]
PW8	Oct-15	100.3	2.3	19.9	40.5	5.4	2	< dl	< dl	12.8	0.007	1.25	*0.04*	1	−2.3	−2.5
PW8	Apr-16	51.9	1.3	9.54	23.5	5.4	5.5	14.5	0.43	10.7	0.0118	1.18	*0.03*	1	−2.5	−2.5
UPC	Apr-16	8.4	0.6	1.47	6.116	10.0	215	134	0.84	0.29	0.043	0.8	0.3	2	−4.6	−2.7
PH Spring	Apr-16	50.9	0.5	6.45	21.8	7.0	4.8	11.5	0.083	0.787	< dl	2.91	*0.04*	1	−3.6	N/A[c]
PH Toe	Oct-14	235	3.7	69.3	144	6.6	39,900	40	22,000	5.9	2.1	1.73	*0.05*	1	−2.6	−0.4
PH Toe	Oct-15	225	3.7	77.3	149	< dl	36,800	69	17,900	3.9	2.1	1.64	*0.05*	3	−2.8	−0.5
PH Toe	Apr-16	288	4.0	116	168	< dl	124,700	267	39,700	10.84	6.81	1.93	0.09	4	−2.5	0.1
Buckskin Catchment																
BW1	Apr-16	20.4	0.68	2.95	34.1	5.69	4.2	127	16.8	16.0	< dl	0.94	*0.04*	1	−2.6	N/A[c]
BW3	Oct-14	31.5	0.31	6.65	22.04	5.2	< dl	22	20.4	22.9	< dl	0.87	0.04	3	−2.3	N/A[c]
BW3	Oct-15	36.8	0.7	7.93	23.7	3.0	< dl	25	15	22.5	0.014	0.9	*0.1*	3	−2.2	−3.2
BW4	Oct-15	249	4.3	30.4	185	3.9	120	< dl	< dl	27.1	0.01	1.94	*0.04*	1	−1.9	−2.7
BW4	Apr-16	57.2	2.4	6.83	76.2	5.4	2.0	9	0.10	25.2	< dl	1.53	*0.03*	1	−2.1	N/A[c]
BuckC	Oct-14	321	5.69	33.6	287	7.8	12	30	2.0	58	< dl	1.90	0.02	3	−1.5	N/A[c]
BuckC	Oct-15	318	6.1	36.0	275.5	3.3	< dl	30	33	61	0.02	1.90	*0.03*	1	−1.5	−2.9
BuckC	Apr-16	263	5.1	28.5	259	6.2	2.1	47	2.0	79.0	< dl	1.71	0.05	2	−1.4	N/A[c]
BuckSpring	Apr-16	38.1	0.8	6.7	7.3	7.4	9.7	15.2	1.63	2.17	0.0052	0.95	*0.03*	1	−3.2	−4.1
Process Water and Pit Wall Runoff																
PD-14	Oct-14	20.3	0.6	0.147	113.3	6.0	100	84	6	341	0.32	0.69	0.03	3	−1.4	−1.3
TP-14	Oct-14	648	54.9	37.4	325	< dl	60	54	7,030	3,260	0.9	0.58	0.02	3	0.4	1.1
Other Nearby Catchments																
TC4	Oct-14	14.2	0.6	2.39	5.2	9.28	0.8	3	< dl	1.2	0.04	1.20	0.03	3	−3.8	−2.4
TC4	Oct-15	15.3	0.7	2.57	5.24	5.1	4	< dl	< dl	< dl	0.005	1.22	*0.06*	1	−3.6	−2.6
TCg	Oct-14	25.2	0.7	5.76	9.3	7.5	24	4.9	< dl	2.2	< dl	1.48	0.03	3	−3.3	N/A[c]
TCg	Oct-15	29.7	0.8	7.05	10.3	5.1	2	< dl	< dl	0.6	< dl	1.47	*0.05*	1	−3.2	N/A[c]
Sunbeam	Apr-16	1.73	2.3	< dl	87	39	235	1	2.81	23.9	< dl	1.00	*0.06*	1	−3.5	N/A[c]
BC3A	Oct-15	74	1.9	23.2	1.3	0.7	< dl	352	37	4.9	0.016	1.53	*0.04*	1	−2.7	−3.2

– Indicates that the parameter was not analyzed; < dl indicates below detection limit.
The highest significant digit in the 2 SD of each measurement was used to define the number of significant digits shown in Table 3B.
[a] δ^{98}Mo expressed relative to NIST-SRM-3134 = +0.25‰.
[b] 2 SD for duplicate or triplicate analysis on the MC-ICP-MS. For samples that were analyzed only once, 2 SE is shown and denoted by italic font.
[c] Saturation index calculation was not possible because one of the required elements was below detection limit.

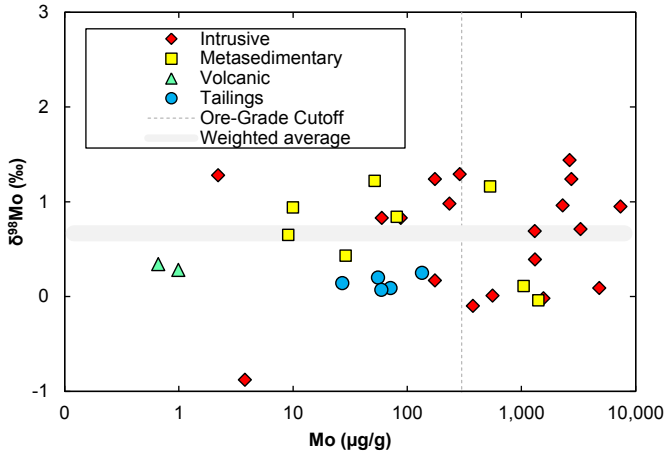

Fig. 2. Molybdenum isotopic composition and Mo contents of waste rock, ore, and mine tailings samples. The horizontal gray shading represents the average Mo isotopic composition, weighted by Mo concentration, for the entire sample set. 2 SD error bars are smaller than symbol sizes.

and Gao, 2013) and its δ^{98}Mo of 0.3–0.4‰ (Voegelin et al., 2014). The Mo content in a sample of massive pyrite found in waste rock (PH-IW-16-1 Py) was also low at 0.165 µg/g (Table 2), in agreement with a recent study showing that pyrite is not an important host of Mo in igneous sulfides (Greaney et al., 2016). Mine tailings samples represent homogenized ore-grade intrusive and metasedimentary rock with minor quantities of residual sulfides, including pyrite, marcasite, pyrrhotite, and molybdenite (Lorax Environmental Services Ltd., 2011b). The average δ^{98}Mo of tailings was homogenous at 0.1 ± 0.1‰ (2 SD, n = 5). In contrast, intrusive and metasedimentary rock samples had more elevated Mo contents spanning from 0.4 to > 7000 µg/g and variable δ^{98}Mo values ranging from -0.9 to 1.3‰ (Fig. 2). Variation of Mo isotopic compositions within a single deposit is typical and is thought to be caused by redox changes and Rayleigh-type fractionation during the precipitation of molybdenite from hydrothermal vapors (Greber et al., 2014; Hannah et al., 2007; Mathur et al., 2010; Skierszkan et al., 2016).

Given the variability in solid-phase δ^{98}Mo, an estimate for the isotopic signature of Mo entering mine drainage from molybdenite oxidative dissolution at the scale of the site's WRSFs was calculated by averaging the δ^{98}Mo value, weighted by Mo abundance, in all waste rock, tailings, and ore samples. Samples from Step 2 in the sequential chemical extractions were included in this weighted average calculation because they represented molybdenite mineralization, as demonstrated by their elevated average Mo content, which exceeded 1500 µg/g, and XRD characterization (Supplementary Tables S6 and S8). The weighted average δ^{98}Mo of waste rock, tailings and ore—hereafter referred to as “mine-waste Mo”—was 0.7 ± 1.0‰ (abundance-weighted

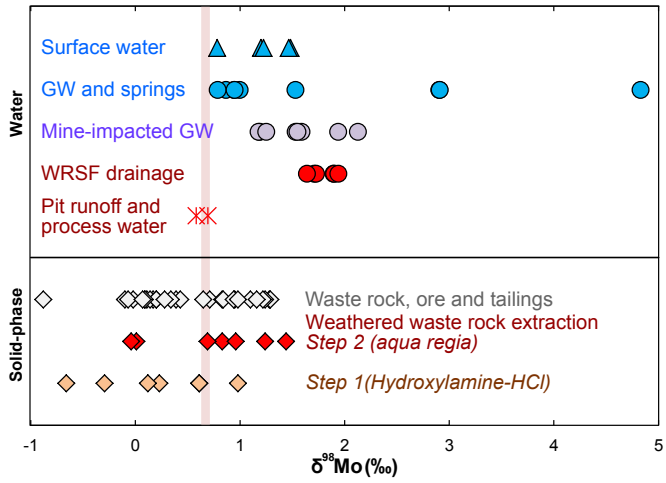

Fig. 3. Molybdenum isotopic compositions of water samples (above) and solid-phase samples (below). GW = groundwater, WRSF = waste-rock storage facility. Weathered waste rock extractions refer to sequential chemical extractions as described in section 3.3. Step 1 represents Mo leached under soluble and reducible aqueous conditions; Step 2 represents Mo leached under oxidizable conditions. The vertical shaded area represents the average δ^{98}Mo weighted by Mo abundance in waste rock, ore and tailings. Error bars are smaller than the symbol sizes.

2 SD, n = 36).

4.2. Source characterization: process water and pit wall runoff

Mine process water (sample TP-14) and runoff collected in the mine's open pit (sample PD-14, Table 1) constituted end-member source waters representing MoS_2 oxidative dissolution (*i.e.,* prior to significant Mo attenuation reactions). As a result of extensive interaction with molybdenite, these water samples had Mo concentrations orders of magnitude higher (3260 µg/L and 341 µg/L, respectively) in comparison with other mine drainage, surface water, and groundwater samples (Table 3). The δ^{98}Mo of the process water and pit runoff ranged from 0.6 to 0.7‰ and was therefore isotopically indistinguishable from the mine-waste Mo. Process water and pit runoff were also isotopically lighter than all other water samples, which spanned from 0.8 to 4.8‰ (Fig. 3).

4.3. Groundwater, surface water and WRSF drainage

Groundwater, surface water, and WRSF drainage samples ranged from 0.6 to 4.8‰ (Fig. 3). Despite marked differences in the aqueous chemistry between the acidic Pat Hughes WRSF and the alkaline Buckskin WRSF, δ^{98}Mo in drainage from both WRSFs fell within a relatively narrow and isotopically heavy range of 1.6–1.9‰. Sulfide mineral oxidation caused sulfate concentrations in Pat Hughes and Buckskin waste-rock drainages to exceed 1100 mg/L (Table 3). However, alkaline drainage from the Buckskin WRSF at BuckC (pH 7.6 to 8.0) had close to ten times higher Mo concentrations than drainage from the acidic Pat Hughes WRSF at PH Toe (pH 4.4 to 4.9), which had < 12 µg/L Mo.

4.3.1. Buckskin Creek Catchment

Within the Buckskin Creek Catchment, WRSF drainage (BuckC) contained in excess of 1100 mg/L sulfate and 58 to 79 µg/L Mo with a δ^{98}Mo that was distinctly isotopically heavy (1.7–1.9‰). In contrast, groundwater and spring samples unimpacted by mining (BW1, BW3, and Buckspring) in the Buckskin Catchment had < 59 mg/L SO_4^{2-}, < 23 µg/L Mo, and an average δ^{98}Mo of 0.9 ± 0.1‰ (2 SD, n = 4) (Table 3 and Fig. 4). In the shallow colluvial/alluvial aquifer immediately downgradient of BuckC, a change in water chemistry at groundwater well BW4 was observed following the installation of a cutoff wall to intercept leakage of mine drainage: In the fall of 2015, 12 months after the wall installation, water at BW4 had δ^{98}Mo (1.9‰) and SO_4^{2-} (921 mg/L) similar to BuckC mine drainage; however, by the spring of 2016, its δ^{98}Mo and SO_4^{2-} had decreased to 1.5‰ and 205 mg/L, respectively. Molybdenum concentrations remained close to 25 µg/L at BW4 throughout this time.

4.3.2. Pat Hughes Creek Catchment

In comparison with the narrow range of δ^{98}Mo in unimpacted water within the Buckskin Creek Catchment, groundwater and surface water samples in the Pat Hughes Creek Catchment were more variable, spanning from 0.8 to 4.8‰ (Table 3 and Fig. 4). This range fully encompassed the isotopic composition of Pat Hughes WRSF drainage monitored at PH Toe, which was 1.6–1.9‰. The δ^{98}Mo in shallow groundwater and surface water (represented by PW7, PW8, and UPC) spanned from 0.8 to 1.6‰ and was therefore isotopically lighter than deep groundwater and a spring (represented by PW10 and PW13 and PH Spring); these had δ^{98}Mo values of 2.9–4.8‰ and Mo concentrations that were < 2 µg/L. Molybdenum concentrations in unimpacted groundwater (PW10 and PW13) and surface water (UPC) were 1–2 orders of magnitude lower in the Pat Hughes Creek Catchment than those in the Buckskin Creek Catchment.

The Mo content in the white precipitate forming at the outflow of the Pat Hughes WRSF was 39.8 µg/g, and its δ^{98}Mo was 1.0‰ (Supplementary Table S7). This δ^{98}Mo was 0.6–0.9‰ lighter than the values observed in WRSF drainage at PH Toe, demonstrating Mo isotopic fractionation between the drainage and the precipitate. Its mineralogy could not be identified using X-ray diffraction or Raman spectroscopy due to its amorphous and nanocrystalline structure, although analyses by ICP-MS (this study) and previous SEM-EDS work (Lorax Environmental Services Ltd., 2011c) indicated that it is composed principally of Al, S, and O and therefore likely to be amorphous aluminum sulfate or hydroxysulfate. Aluminum sulfates are known to precipitate in acidic and sulfate-rich waters (Nordstrom, 1982) and have been observed to form amorphous white precipitates where acid-sulfate and alkaline waters mix (Munk et al., 2002; Theobald et al., 1963). These processes are analogous to those at PH Toe where groundwater discharge mixes with Pat Hughes WRSF drainage.

4.4. Characterization of weathered waste-rock surfaces

XRD showed that molybdenite was present in all of the surface scrapings of weathered waste rock that were subjected to sequential chemical extractions (Supplementary Table S8). Jarosite and gypsum were also present in three and four of the seven samples, respectively. Poorly crystalline Fe-(oxy)hydroxides forming in mine waste-rock environments are typically not detectable using XRD (Das and Hendry, 2011) and were not identified by XRD scans. Secondary molybdate minerals (*e.g.,* powellite and wulfenite) were also not observed.

The chemical sequential extraction results indicated an accumulation of Fe-(oxy)hydroxides and sulfate minerals on waste-rock coatings. Iron was the most abundant cation in Step 1 (NH_2OH-HCl/HCl), ranging from 1 to 9 wt %, while total sulfur contents ranged from 0.2 to 1 wt % (Supplementary Table S6). Molybdenum contents in Step 1 ranged from 19 to 202 µg/g with an average of 96 µg/g (Fig. 5 and Supplementary Table S6). Proportionally, a much larger amount of Mo was recovered in the *aqua regia* digestion of the residues (Step 2) as a result of the presence molybdenite in the samples (Fig. 5). The δ^{98}Mo in Step 1 was depleted in heavy Mo isotopes in comparison with waste rock and mine water samples (Fig. 3). It was also isotopically lighter compared with the Mo extracted in Step 2 in five of the seven samples (Fig. 5).

5. Discussion

The span in δ^{98}Mo among samples in this study was 5.7‰, which

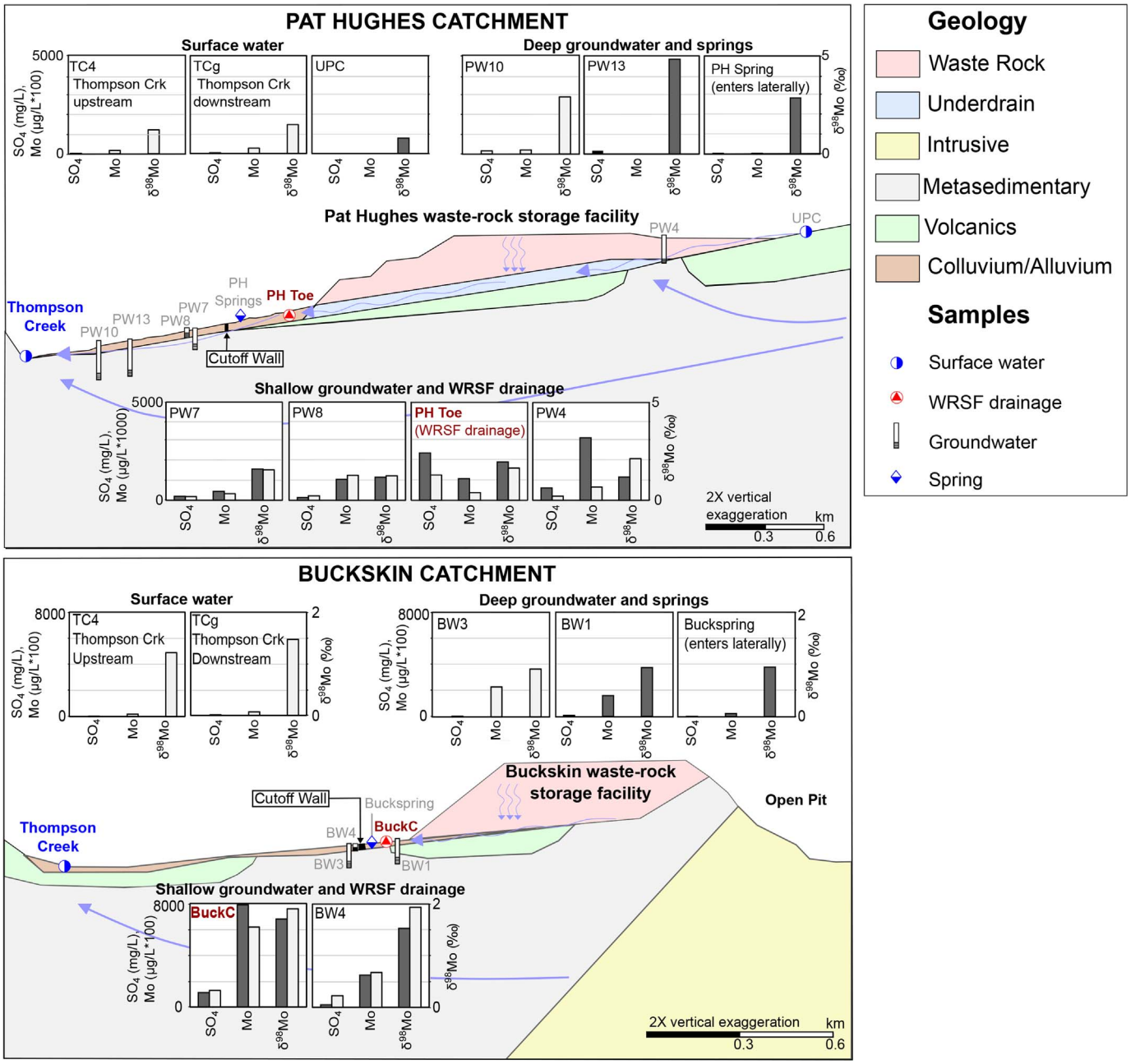

Fig. 4. Cross-sectional views along the catchments of Pat Hughes Creek (above) and Buckskin Creek (below) showing concentrations of Mo and SO_4^{2-} and $\delta^{98}Mo$ in water samples. SO_4^{2-} and Mo are plotted against left-hand y-axis in bar graphs (units mg/L and µg/L x 100, respectively); $\delta^{98}Mo$ is plotted against right-hand y-axis (units ‰). Note that y-axis scales are different between the cross-sections. TC4 and TCg samples are from Thompson Creek, upstream and downstream of the confluences with Buckskin and Pat Hughes Creeks. Dark gray shading in bar plots represents spring 2016 samples; light gray shading shows fall 2015 samples. WRSF = waste-rock storage facility. Hydrostratigraphy modified from Lorax Environmental Services Ltd. (2011a).

nearly encompasses the range of 6.4‰ compiled from natural and environmental samples measured to date (Goldberg et al., 2013). The average $\delta^{98}Mo$ in WRSF drainage sampled at BuckC and PH Toe of 1.8 ± 0.3‰ (2 SD, n = 6) was isotopically heavy in comparison with mine-waste Mo (0.7‰) and the Mo released in Step 1 of our chemical extraction, which averaged 0.2 ± 1.1‰ (2 SD, n = 7). The increase of $\delta^{98}Mo$ in water relative to rocks corroborated studies of natural and contaminated environments that demonstrated an enrichment of heavy Mo isotopes in aqueous solutions during weathering and transport (Kendall et al., 2017; King et al., 2016; Pearce et al., 2010; Siebert et al., 2015; Skierszkan et al., 2016; Voegelin et al., 2012). This fractionation follows the chronological sequence of molybdenite oxidative dissolution and subsequent attenuation reactions that lead to molybdate removal from solution via adsorption or mineral precipitation. Molybdenum isotopic fractionation in WRSF drainage must therefore arise from either molybdenite dissolution or attenuation reactions or from a combination of these processes.

5.1. Absence of isotopic fractionation from molybdenite dissolution

Pit wall runoff and mine process water samples PD-14 and TP-14 serve as analogs for the geochemical composition of solutions after molybdenite oxidative dissolution. Both of these waters underwent extensive interaction with molybdenite, as shown by their Mo concentrations ranging from 341 to 3260 µg/L. These Mo concentrations were orders of magnitude higher than in all other water samples, which

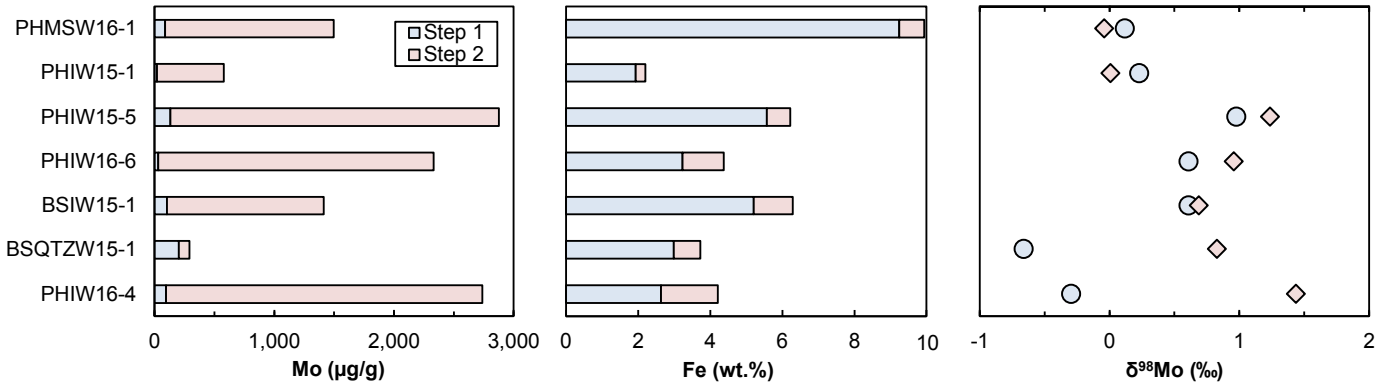

Fig. 5. Molybdenum (left) and Fe (center) contents and Mo isotopic compositions (right) from sequential chemical extractions of weathered waste rock. Blue shading: Step 1 = 1M NH_2OH-HCl/1 M HCl; red shading: Step 2 = *Aqua regia*. See section 3.3 for full details of extraction procedure. 2 SD error bars on Mo isotopic compositions are smaller than symbol sizes. (For interpretation of the references to colour in this figure legend, the reader is referred to the web version of this article.)

had 0.3 to 79 µg/L Mo (Table 3). The isotopic compositions of PD-14 and TP-14 were equal within 0.1‰ to mine-waste Mo, suggesting that at large spatial scales, isotopic fractionation from molybdenite oxidative weathering in the absence of Mo attenuation is negligible. Among all the water samples collected at the site, PD-14 and TP-14 constituted an end-member with the highest Mo concentration and isotopically lightest δ^{98}Mo. This result is consistent with a global survey of δ^{98}Mo in rivers, whose end-member with the highest Mo concentration (49 µg/L) and lightest δ^{98}Mo (0.2‰) was a creek receiving Mo-rich mine drainage (Clear Creek, Colorado, USA; Archer and Vance, 2008). Other field and laboratory studies have also found limited Mo isotope fractionation as a result of the oxidative dissolution process (Pearce et al., 2010; Siebert et al., 2015, 2003; Voegelin et al., 2012). In contrast, all other groundwater, surface water, and mine drainage had heavier δ^{98}Mo values spanning 0.8 to 4.8‰ and significantly lower Mo concentrations, which ranged from 0.3 to 79 µg/L. These observations suggest that Mo attenuation processes occurring after molybdenite dissolution are largely responsible for the shift toward heavy δ^{98}Mo compositions during Mo removal.

5.2. Evidence for the role of adsorption in controlling Mo mobility in waste rock

Given the apparent lack of Mo isotope fractionation during molybdenite oxidative dissolution, the isotopically heavy δ^{98}Mo of 1.6–1.9‰ in mine drainage at BuckC and PH Toe relative to mine-waste Mo can be explained only by an alternative source of isotopically heavy Mo or by enrichment in heavy Mo isotopes in solution as a result of Mo removal or by a combination of these processes.

Examining water-sample data in plots of δ^{98}Mo against Mo/SO_4^{2-} provides support for the occurrence of Mo removal processes. δ^{98}Mo and Mo/SO_4^{2-} are useful tracers of Mo attenuation along a reactive flowpath: Initial oxidation of molybdenite should produce a source-term water with high Mo/SO_4^{2-} and a δ^{98}Mo similar to mine-waste Mo. Subsequent aqueous molybdate adsorption would decrease Mo/SO_4^{2-} and increase δ^{98}Mo due to preferential removal of lighter Mo isotopes (Barling and Anbar, 2004; Siebert et al., 2015; Wasylenki et al., 2008). Any precipitation of common sulfate-bearing mine drainage minerals such as gypsum, jarosite, or schwertmannite (Blowes et al., 2014) would increase Mo/SO_4^{2-} with no change in δ^{98}Mo; higher pyrite/molybdenite weathering ratios would decrease Mo/SO_4^{2-}, also without affecting δ^{98}Mo. Both δ^{98}Mo and Mo/SO_4^{2-} measurements are unchanged by dilution.

Assuming that pit wall runoff or process water (samples PD-14 and TP-14) are representative of a source-term end-member (high Mo/SO_4^{2-} with isotopically light δ^{98}Mo), drainage samples from both WRSFs fit an attenuation trend, wherein mine drainage is shifted to low Mo/SO_4^{2-} with isotopically heavy δ^{98}Mo as a result of Mo removal (Fig. 6). Unimpacted groundwater in the Buckskin Catchment occupies intermediate compositions in the δ^{98}Mo-Mo/SO_4^{2-} space, more closely reflecting direct molybdenite dissolution (with limited Mo attenuation). The remarkably heavy δ^{98}Mo of > 2.9‰ observed in select groundwater samples from the Pat Hughes Catchment (*i.e.,* PW10 and PW13) is associated with deep sulfidic and ferruginous groundwater from the metasedimentary bedrock aquifer, with low Mo concentrations of < 2 µg/L. Upward hydraulic gradients and low sulfate concentrations at depth suggest that these waters are not affected by mine drainage and could represent a highly fractionated residual pool of aqueous Mo after redox-driven removal processes in the deep aquifer: These groundwaters were at FeS saturation with saturation indices ranging from 0.09 to -0.05, and various studies report that Mo is effectively precipitated out of sulfidic and ferruginous aqueous solutions (Helz et al., 2011, 1996; Vorlicek et al., 2004). This process also favors the enrichment of heavy Mo isotopes in residual aqueous Mo (Dahl et al., 2010; Nägler et al., 2011; Neubert et al., 2008; Tossell, 2005).

Characterization of surface scrapings on weathered waste rock collected by sequential chemical extractions and X-ray diffraction (XRD) provides evidence that Mo adsorption is the process responsible for the fractionation of δ^{98}Mo in WRSF drainage. Recall that Mo contents recovered in Step 1 (NH_2OH-HCl/HCl) of the sequential extractions represent a lower bound for adsorbed Mo on mineral surface coatings due to the entrainment of primary silicate and sulfide grains. The average Mo content in Step 1 of 96 µg/g therefore shows an association of Mo with minerals that dissolved in the reducing NH_2OH-HCl/HCl environment, presumably Fe-(oxy)hydroxides and soluble (hydroxy)sulfates. The average δ^{98}Mo of this pool of molybdenum is 0.2 ± 1.1‰ (2 SD, n = 7) and therefore isotopically light relative to WRSF drainage, which ranges from 1.6 to 1.9‰ (Fig. 3). This fractionation is consistent with laboratory studies showing enrichment of isotopically light Mo isotopes in adsorbed phases (Barling and Anbar, 2004; Goldberg et al., 2009; Wasylenki et al., 2008). Furthermore, if the majority of the Mo released from molybdenite weathering were retained in adsorbed phases, isotopic mass balance dictates that their isotopic composition should be similar to that of mine-waste Mo at 0.7‰, which fits with the observed data.

The molybdate minerals powellite and wulfenite are also plausible Mo sinks in oxidized mining waste rock (Conlan et al., 2012), but these are unlikely to be forming in the WRSFs studied here. Molybdenum concentrations are more than one order of magnitude below the threshold required for powellite saturation (Table 3), and wulfenite formation requires aqueous Pb^{2+}, whose content is much lower in geologic samples (0.4–45 µg/g, data not shown) compared with Mo concentrations and which readily precipitates from aqueous solutions in the presence of common anions such as OH^-, HCO_3^- and SO_4^{2-} (Hirsche et al., 2017). Molybdate minerals were also not detected by XRD scans in weathered waste-rock samples.

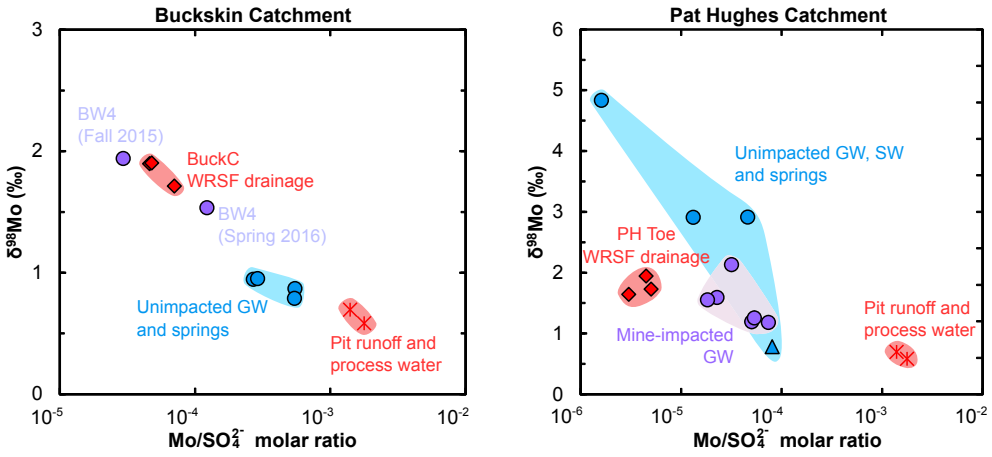

Fig. 6. Molybdenum isotopic ratios against Mo/SO_4^{2-} molar ratios in samples from the Buckskin Creek Catchment (left) and the Pat Hughes Catchment (right). Note differences y- and x-axis scales between graphs. Pit wall runoff and mine process water samples represent the initial geochemical signature of Mo-rich waters resulting from primary molybdenite dissolution. WRSF = waste-rock storage facility, GW = groundwater, SW = surface water. Symbols indicate water type: diamonds = WRSF drainage, circles = groundwater and springs, triangles = surface water, crosses = pit runoff and process water. Groundwater sample symbol color indicates mining effects: blue = unimpacted by mining, purple = impacted. (For interpretation of the references to colour in this figure legend, the reader is referred to the web version of this article.)

Groundwater discharge constitutes a possible alternative source of Mo to drainage collected at the base of WRSFs, but it is also unlikely to explain the heavy Mo isotopic signature at BuckC and PH Toe. In the Buckskin Creek Catchment, all groundwater and spring samples unimpacted by mining had Mo concentrations < 23 µg/L and δ^{98}Mo of 0.9–1.0‰, while BuckC mine drainage contained 58 to 79 µg/L Mo and had a δ^{98}Mo of 1.7–1.9‰ (Fig. 4). In the Pat Hughes Creek Catchment, unimpacted groundwater, surface water, and spring samples (PW10, PW13, UPC, and PH Spring) had a broader range in δ^{98}Mo that spanned from 0.8 to 4.8‰ (Fig. 4). However, the Mo concentrations in these samples were exceedingly low at < 2 µg/L. In addition, during fall sampling at PH Toe, when the groundwater contribution to mine drainage is maximal, δ^{98}Mo values were 0.2–0.3‰ lighter than samples collecting during spring freshet (when the groundwater contribution is smallest), further indicating that groundwater was unlikely to be the source of heavy δ^{98}Mo in the Pat Hughes WRSF drainage.

5.3. Molybdenum attenuation in alkaline and acidic WRSF drainages

The narrow range of δ^{98}Mo—from 1.6 to 1.9 ‰—in drainage at PH Toe and BuckC, despite a tenfold difference in Mo concentrations and their contrasting pH values, is an intriguing result that merits further discussion. A graphical projection of Mo removal via adsorption onto various mineral surfaces in the δ^{98}Mo-Mo/SO_4^{2-} space provides a mechanism to explain the similarity in δ^{98}Mo of drainage from both WRSFs. Starting from the source-term composition defined by pit wall runoff or process water and applying equilibrium isotopic fractionation factors for Mo adsorption onto Fe-(oxy)hydroxides from the literature (Goldberg et al., 2009), the resulting projections reach a δ^{98}Mo plateau when the Mo/SO_4^{2-} molar ratio decreases below approximately 10^{-4}, corresponding to > 90% Mo removal (Fig. 7). All samples from BuckC and PH Toe fall within the values predicted for equilibrium adsorption onto ferrihydrite and goethite, although the larger uncertainty in the fractionation factor of goethite yields a wider range in predicted δ^{98}Mo values (Goldberg et al., 2009). The large surface area of these minerals acts as an important adsorption surface for molybdate (Brinza et al., 2008), and they are abundant oxidation products in pyritic mine waste-rock under the pH range found in both WRSFs (Blowes et al., 2014). A fractionation factor for Mo incorporation into Al-(hydroxy)sulfates can also be calculated from our δ^{98}Mo measurements of mine drainage and of the Al-(hydroxy)sulfate precipitates at PH Toe. However, δ^{98}Mo data at PH Toe and BuckC fall outside of the range predicted by this process in the δ^{98}Mo-Mo/SO_4^{2-} space (Fig. 7). The fractionation factors for Mo adsorption onto other mineral surfaces that have an affinity for Mo and may be present in WRSFs, such as schwertmannite, clays, and pyrite (Bostick et al., 2003; Goldberg et al., 1996; Antelo et al., 2012), are not known at present. The hypothesis that extensive (> 90%) Mo adsorption onto mineral surfaces explains the similar δ^{98}Mo in drainage from both WRSFs is also consistent with predictions made from isotopic mass balance using results from Step 1 in the sequential chemical extractions, which suggests that a large proportion of liberated Mo is retained on mineral surfaces.

In addition, while the Mo isotopic composition is similar in drainage from both WRSFs, the significantly lower Mo/SO_4^{2-} at PH Toe in comparison with BuckC is consistent with a greater extent of Mo removal in the Pat Hughes WRSF (Fig. 7). This result is expected: The Pat Hughes WRSF contains significantly more molybdenite and pyrite than the Buckskin WRSF, and Mo concentrations at PH Toe had reached tens to hundreds of µg/L prior to becoming persistently acidic in 2006 (Dockrey and Stockwell, 2012). Since 2006, the stabilization of drainage to a pH of approximately 4.5—near the optimum for molybdate adsorption—and a decrease in Mo concentrations to < 10 µg/L provide strong circumstantial evidence that Mo transport is retarded by adsorption (Dockrey and Stockwell, 2012).

The occurrence of a large amount of Mo removal via adsorption in the Buckskin WRSF is unexpected given the alkaline pH of drainage at BuckC. However, approximately 23% of the Buckskin WRSF is composed of potentially acid-generating (PAG) metasedimentary and intrusive waste rock (Dockrey and Stockwell, 2012), which is encapsulated by NAG waste within the WRSF. Zones enriched in PAG waste may therefore generate localized acidic drainage and accumulation of secondary minerals such as Fe-(oxy)hydroxides) from sulfide weathering, which favor Mo adsorption and commensurate isotopic fractionation. Drainage from these acidic zones could be neutralized by mixing with alkaline water generated from the weathering of NAG waste and an influx of groundwater discharge, resulting in an increase of solution pH and transport of the remaining isotopically heavy aqueous Mo to BuckC.

5.4. δ^{98}Mo and Mo/SO_4^{2-} to trace Mo sources in shallow groundwater (BW4)

δ^{98}Mo and Mo/SO_4^{2-} data provided useful tracers of Mo provenance at groundwater well BW4, within the shallow colluvial/alluvial aquifer immediately downgradient of the Buckskin WRSF (Fig. 4). In November 2014, a cutoff wall was installed to intercept leakage of mine drainage into the colluvial/alluvial aquifer, which had the effect of changing the source of groundwater at BW4 from mine drainage to natural groundwater. In October 2015, BW4 showed a strong mine-drainage signature with sulfate concentrations of 921 mg/L compared with natural background water in the Buckskin Catchment that had < 60 mg/L SO_4^{2-}. By April 2016, 17 months after the installation of the cutoff wall, SO_4^{2-} concentrations had decreased to 205 mg/L, and δ^{98}Mo and Mo/SO_4^{2-} values had shifted towards the composition of natural artesian groundwater at BW1 and BW3 (Fig. 6). These changes indicated that the wall was successfully limiting mine drainage infiltration into

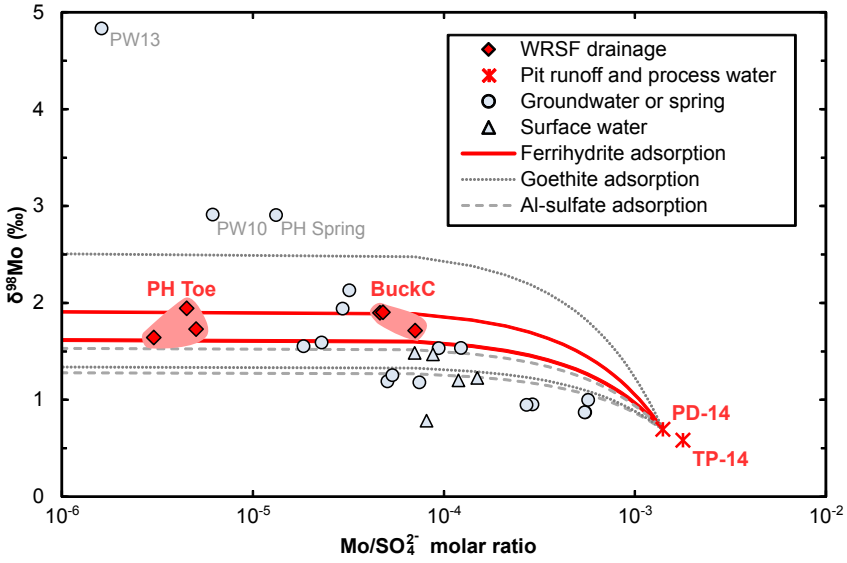

Fig. 7. Molybdenum isotopic ratios against Mo/SO_4^{2-} for all water samples. The curves are graphical projections of equilibrium Mo isotopic fractionation during adsorption onto ferrihydrite, goethite and aluminum hydroxysulfate starting from pit runoff sample PD-14, which represents the initial composition of water after dissolution of sulfidic waste rock. Waste-rock storage facility (WRSF) drainage falls within the projections for Mo adsorption onto ferrihydrite and goethite. The fractionation factors used in the projection of ferrihydrite and goethite adsorption are taken from Goldberg et al. (2009). The fractionation factor for aluminum hydroxysulfate adsorption is calculated from the difference of δ^{98}Mo between the precipitate and the range observed in WRSF drainage at PH Toe (Supplementary Table S7 and Table 3). Curves show the minimal and maximal range in δ^{98}Mo given reported uncertainties associated with the fractionation factors.

colluvial groundwater. This effect would not have been noticeable on the basis of Mo concentrations alone, which were unchanged during this time period. Mo isotopic mass balance calculations using the range of observed δ^{98}Mo values in unimpacted groundwater in the Buckskin Catchment (0.9–1.0‰) and at BuckC (1.7–1.9‰) suggested that 22 to 44% of the Mo at BW4 after installation of the cutoff wall came from BuckC infiltration, with this quantity predicted to decrease as the plume of mine drainage becomes gradually displaced by natural groundwater infiltration.

6. Conclusions

δ^{98}Mo analyses in rock, groundwater, surface water and mine drainage demonstrated that fractionations in excess of 5‰ can be present at a single mine site. This observation indicates that care must be taken to characterize the isotopic composition of these different Mo sources (*e.g.,* groundwater, molybdenites), as they can be spatially variable within the catchment scale. Molybdenum isotopic fractionation appears to be limited during the oxidative dissolution of molybdenite in mine waste rock: Mo-rich (> 340 μg/L) mine process water and pit wall runoff had δ^{98}Mo values that were within 0.1‰ of the average δ^{98}Mo of mine-waste Mo (waste rock, tailings and ore), which was 0.7 ± 1.0‰ (average and 2 SD weighted by Mo abundance, n = 36). Prior to any Mo attenuation process, the δ^{98}Mo of aqueous molybdate therefore reflected the isotopic composition of the source of Mo, which was molybdenite-bearing waste rock.

δ^{98}Mo in alkaline and acidic mine drainage from the bases of two large (> 130 million tons) waste-rock storage facilities (WRSF) ranged from 1.6 to 1.9‰ and was therefore enriched in heavy Mo isotopes relative to mine-waste Mo. This fractionation indicates that the relatively low Mo concentrations of 4–79 μg/L in mine drainage result from Mo attenuation rather than a lack of Mo release. The dominant Mo attenuation process is adsorption onto mineral surfaces, as demonstrated by two lines of evidence: (1) the accumulation of isotopically light Mo in secondary minerals collected from the surfaces of weathered waste rock and (2) the increase of δ^{98}Mo and decrease of Mo/SO_4^{2-} in drainage from the base of WRSFs relative to Mo-rich source waters (pit runoff and process water) resulting from molybdenite oxidative dissolution. The occurrence of Mo adsorption in a WRSF generating alkaline mine drainage suggests that localized areas of depressed pH are likely present within the WRSF because acidic conditions are required to promote Mo adsorption (Goldberg et al., 1996). δ^{98}Mo can therefore constitute a tracer of small-scale mine-drainage acidification, a process that is not captured by monitoring only Mo concentrations and pH in outflow WRSF drainage. The minerals providing adsorption surfaces in weathered waste-rock are most likely Fe-(oxy)hydroxides from pyrite weathering. Attenuated Mo should remain stable as long as the waste-rock environment remains oxidized (*i.e.,* unsaturated and uncovered) and pH does not drop below 4, such that Fe-(oxy)hydroxides do not dissolve.

δ^{98}Mo data used in conjunction with Mo/SO_4^{2-} also served as a useful tracer of groundwater remediation in a shallow aquifer after the installation of a cutoff wall to prevent mine drainage leakage. Altogether, Mo isotope ratio measurements constitute an effective indicator of processes controlling Mo mobility during the weathering of molybdenite-rich waste rock. This approach should become increasingly powerful as the mechanisms of Mo stable isotope fractionations become unraveled through more research in both field and experimental settings.

Acknowledgements

The Thompson Creek Metals Company and, in particular, Richard Giampedraglia, Bert Doughty, Ray Cheff and Chris Natoli are warmly thanked for providing support with field site access, equipment and logistics. Mine staff support was critical to the completion of this work. Maureen Soon, Dr. Marghaleray Amini and Kathy Gordon are thanked for assistance with ICP-OES, ICP-MS and MC-ICP-MS analyses. Dr. Elisabetta Pani, Lan Kato and Jenny Lai assisted with X-ray diffraction analyses. This research was possible thanks to generous financial support from Lorax Environmental Services, NSERC MAGNET and a NSERC Canada Graduate Scholarship Grant to EKS.

Appendix A. Supplementary data

Supplementary data related to this article can be found at http://dx.doi.org/10.1016/j.apgeochem.2017.10.008.

References

Antelo, J., Fiol, S., Gondar, D., López, R., Arce, F., 2012. Comparison of arsenate, chromate and molybdate binding on schwertmannite: Surface adsorption vs anion-exchange. J. Colloid Interface Sci. 386, 338–343. http://dx.doi.org/10.1016/j.jcis.2012.07.008.

Archer, C., Vance, D., 2008. The isotopic signature of the global riverine molybdenum flux and anoxia in the ancient oceans. Nat. Geosci. 1, 597–600. http://dx.doi.org/10.1038/ngeo282.

Axelsson, M.D., Rodushkin, I., Ingri, J., Ohlander, B., 2002. Multielemental analysis of Mn-Fe nodules by ICP-MS: optimisation of analytical method. Analyst 127, 76–82. http://dx.doi.org/10.1039/b105706p.

Barceloux, D.G., 1999. Molybdenum. Clin. Toxicol. 37, 231–237.
Barling, J., Anbar, A.D., 2004. Molybdenum isotope fractionation during adsorption by manganese oxides. Earth Planet. Sci. Lett. 217, 315–329. http://dx.doi.org/10.1016/S0012-821X(03)00608-3.
Blowes, D., Ptacek, C.J., Jambor, J.L., Weisener, C., Paktunc, D., Gould, W., Johnson, D., 2014. The geochemistry of acid-mine drainage. In: Holland, H.D., Turekian, K.K. (Eds.), Treatise on Environmental Geochemistry, eleventh ed. Elsevier, pp. 131–190. http://dx.doi.org/10.1016/B978-0-08-095975-7.00905-0.
Bostick, B.C., Fendorf, S., Helz, G.R., 2003. Differential adsorption of molybdate and tetrathiomolybdate on pyrite (FeS2). Environ. Sci. Technol. 37, 285–291. http://dx.doi.org/10.1021/es0257467.
Brinza, L., Benning, L.G., Statham, P.J., 2008. Adsorption studies of Mo and V onto ferrihydrite. Mineral. Mag. 72, 385–388. http://dx.doi.org/10.1180/minmag.2008.072.1.385.
Chappaz, A., Lyons, T.W., Gregory, D.D., Reinhard, C.T., Gill, B.C., Li, C., Large, R.R., 2014. Does pyrite act as an important host for molybdenum in modern and ancient euxinic sediments? Geochim. Cosmochim. Acta 126, 112–122. http://dx.doi.org/10.1016/j.gca.2013.10.028.
Conlan, M.J.W., Mayer, K.U., Blaskovich, R., Beckie, R.D., 2012. Solubility controls for molybdenum in neutral rock drainage. Geochem. Explor. Environ. Anal. 12, 21–32. http://dx.doi.org/10.1144/1467-7873/10-RA-043.
Connelly, J.N., Ulfbeck, D.G., Thrane, K., Bizzarro, M., Housh, T., 2006. A method for purifying Lu and Hf for analyses by MC-ICP-MS using TODGA resin. Chem. Geol. 233, 126–136. http://dx.doi.org/10.1016/j.chemgeo.2006.02.020.
Dahl, T.W., Anbar, A.D., Gordon, G.W., Rosing, M.T., Frei, R., Canfield, D.E., 2010. The behavior of molybdenum and its isotopes across the chemocline and in the sediments of sulfidic Lake Cadagno, Switzerland. Geochim. Cosmochim. Acta 74, 144–163. http://dx.doi.org/10.1016/j.gca.2009.09.018.
Das, S., Hendry, M.J., 2011. Application of Raman spectroscopy to identify iron minerals commonly found in mine wastes. Chem. Geol. 290, 101–108. http://dx.doi.org/10.1016/j.chemgeo.2011.09.001.
Dockrey, J.W., Stockwell, J.S., 2012. Early indicators of acid seepage generation – a comparative study of long-term seepage quality from two waste rock dumps in the central Rocky mountains. In: Proceedings of the 9th International Conference on Acid Rock Drainage, May 20–25, Ottawa, Canada.
Dragovich, D., 2006. Microchemistry of small desert varnish samples, western new south wales. Australia 23, 445–453.
Essilfie-Dughan, J., Pickering, I.J., Hendry, M.J., George, G.N., Kotzer, T., 2011. Molybdenum speciation in uranium mine tailings using X-ray absorption spectroscopy. Environ. Sci. Technol. 45, 455–460. http://dx.doi.org/10.1021/es102954b.
Goldberg, S., Forster, H.S., Godfrey, C.L., 1996. Molybdenum adsorption on oxides, clay minerals, and soils. Soil Sci. Soc. Am. J. 60, 425–432. http://dx.doi.org/10.2136/sssaj1996.03615995006000020013x.
Goldberg, T., Archer, C., Vance, D., Poulton, S.W., 2009. Mo isotope fractionation during adsorption to Fe (oxyhydr)oxides. Geochim. Cosmochim. Acta 73, 6502–6516. http://dx.doi.org/10.1016/j.gca.2009.08.004.
Goldberg, T., Gordon, G., Izon, G., Archer, C., Pearce, C.R., McManus, J., Anbar, A.D., Rehkämper, M., 2013. Resolution of inter-laboratory discrepancies in Mo isotope data: an intercalibration. J. Anal. At. Spectrom. 28, 724–735. http://dx.doi.org/10.1039/c3ja30375f.
Goumih, A., El Adnani, M., Hakkou, R., Benzaazoua, M., 2013. Geochemical behavior of mine tailings and waste rock at the abandoned Cu-Mo-W azegour mine (occidental high atlas, Morocco). Mine Water Environ. 32, 121–132. http://dx.doi.org/10.1007/s10230-013-0221-0.
Greaney, A.T., Rudnick, R.L., Gaschnig, R.M., 2016. Crustal sources of molybdenum. In: Goldschmidt Conference, June 2016, Yokohama, Japan.
Greber, N.D., Pettke, T., Nägler, T.F., 2014. Magmatic–hydrothermal molybdenum isotope fractionation and its relevance to the igneous crustal signature. Lithos 190–191, 104–110. http://dx.doi.org/10.1016/j.lithos.2013.11.006.
Gustafsson, J.P., 2003. Modelling molybdate and tungstate adsorption to ferrihydrite. Chem. Geol. 200, 105–115. http://dx.doi.org/10.1016/S0009-2541(03)00161-X.
Hannah, J.L., Stein, H.J., Wieser, M.E., de Laeter, J.R., Varner, M.D., 2007. Molybdenum isotope variations in molybdenite: vapor transport and Rayleigh fractionation of Mo. Geology 35, 703–706. http://dx.doi.org/10.1130/G23538A.1.
Helz, G.R., Bura-Nakić, E., Mikac, N., Ciglenečki, I., 2011. New model for molybdenum behavior in euxinic waters. Chem. Geol. 284, 323–332. http://dx.doi.org/10.1016/j.chemgeo.2011.03.012.
Helz, G.R., Miller, C.V., Charnock, J.M., Mosselmans, J.F.W., Pattrick, R.A.D., Garner, C.D., Vaughan, D.J., 1996. Mechanism of molybdenum removal from the sea and its concentration in black shales: EXAFS evidence. Geochim. Cosmochim. Acta 60, 3631–3642. http://dx.doi.org/10.1016/0016-7037(96)00195-0.
Hirsche, D.T., Blaskovich, R., Mayer, K.U., Beckie, R.D., 2017. A study of Zn and Mo attenuation by waste-rock mixing in neutral mine drainage using mixed-material field barrels and humidity cells. Appl. Geochem. 84, 114–125. http://dx.doi.org/10.1016/j.apgeochem.2017.06.005.
Kaback, D.S., Runnells, D.D., 1980. Geochemistry of molybdenum in some stream sediments and waters. Geochim. Cosmochim. Acta 44, 447–456. http://dx.doi.org/10.1016/0016-7037(80)90043-5.
Kendall, B., Dahl, T.W., Anbar, A.D., 2017. The stable isotope geochemistry of molybdenum. Rev. Mineral. Geochem. 82, 683–732. http://dx.doi.org/10.2138/rmg.2017.82.16.
King, E.K., Thompson, A., Chadwick, O.A., Pett-Ridge, J.C., 2016. Molybdenum sources and isotopic composition during early stages of pedogenesis along a basaltic climate transect. Chem. Geol. http://dx.doi.org/10.1016/j.chemgeo.2016.01.024.
Lorax Environmental Services Ltd, 2011a. Thompson Creek Mine – Hydrogeological Assessment of Mine Drainages. 94 p.
Lorax Environmental Services Ltd, 2011b. Thompson Creek Mine Tailings Impoundment – Geochemical Characterization and Water Quality Predictions. 626 p.
Lorax Environmental Services Ltd, 2011c. Thompson Creek Mine Pat Hughes Waste Dump – Geochemical Characterization and Water Quality Predictions. 287 p.
Mathur, R., Brantley, S., Anbar, A., Munizaga, F., Maksaev, V., Newberry, R., Vervoort, J., Hart, G., 2010. Variation of Mo isotopes from molybdenite in high-temperature hydrothermal ore deposits. Min. Depos. 45, 43–50. http://dx.doi.org/10.1007/s00126-009-0257-z.
Munk, L., Faure, G., Pride, D.E., Bigham, J.M., 2002. Sorption of trace metals to an aluminum precipitate in a stream receiving acid rock-drainage; Snake River, Summit County, Colorado. Appl. Geochem. 17, 421–430.
Nägler, T.F., Anbar, A.D., Archer, C., Goldberg, T., Gordon, G.W., Greber, N.D., Siebert, C., Sohrin, Y., Vance, D., 2014. Proposal for an international molybdenum isotope measurement standard and data representation. Geostand. Geoanalytical Res. 38, 149–151. http://dx.doi.org/10.1111/j.1751-908X.2013.00275.x.
Nägler, T.F., Neubert, N., Böttcher, M.E., Dellwig, O., Schnetger, B., 2011. Molybdenum isotope fractionation in pelagic euxinia: evidence from the modern Black and Baltic Seas. Chem. Geol. 289, 1–11. http://dx.doi.org/10.1016/j.chemgeo.2011.07.001.
Neubert, N., Nägler, T.F., Böttcher, M.E., 2008. Sulfidity controls molybdenum isotope fractionation into euxinic sediments: evidence from the modern Black Sea. Geology 36, 775–778. http://dx.doi.org/10.1130/G24959A.1.
Nordstrom, D.K., 1982. The effect of sulfate on aluminum concentrations in natural waters: some stability relations in the system Al_2O_3-SO_3-H_2O at 298 K. Geochim. Cosmochim. Acta 46, 681–692. http://dx.doi.org/10.1016/0016-7037(82)90168-5.
Parkhurst, D.L., Appelo, C.A.J., 2013. Description of Input and Examples for PHREEQC Version 3 — a Computer Program for Speciation, Batch-reaction, One-dimensional Transport, and Inverse Geochemical Calculations. U.S. Geological Survey Techniques and Methods Book 6, chapter A43, 497 p.
Pearce, C.R., Burton, K.W., von Strandmann, P.A.E.P., James, R.H., Gíslason, S.R., 2010. Molybdenum isotope behaviour accompanying weathering and riverine transport in a basaltic terrain. Earth Planet. Sci. Lett. 295, 104–114. http://dx.doi.org/10.1016/j.epsl.2010.03.032.
Pichler, T., Mozaffari, A., 2015. Distribution and mobility of geogenic molybdenum and arsenic in a limestone aquifer matrix. Appl. Geochem. 63, 623–633. http://dx.doi.org/10.1016/j.apgeochem.2015.08.006.
Rudnick, R.L., Gao, S., 2013. Composition of the continental crust. In: Turekian, K., Holland, H. (Eds.), Treatise on Gechemistry, second ed. Elsevier, pp. 1–51. http://dx.doi.org/10.1016/B978-0-08-095975-7.00301-6.
Schudel, G., Lai, V., Gordon, K., Weis, D., 2015. Trace element characterization of USGS reference materials by HR-ICP-MS and Q-ICP-MS. Chem. Geol. 410, 223–236. http://dx.doi.org/10.1016/j.chemgeo.2015.06.006.
Siebert, C., Nägler, T.F., von Blanckenburg, F., Kramers, J.D., 2003. Molybdenum isotope records as a potential new proxy for paleoceanography. Earth Planet. Sci. Lett. 211, 159–171. http://dx.doi.org/10.1016/S0012-821X(03)00189-4.
Siebert, C., Pett-Ridge, J.C., Opfergelt, S., Guicharnaud, R.A., Halliday, A.N., Burton, K.W., 2015. Molybdenum isotope fractionation in soils: influence of redox conditions, organic matter, and atmospheric inputs. Geochim. Cosmochim. Acta 162, 1–24. http://dx.doi.org/10.1016/j.gca.2015.04.007.
Skierszkan, E.K., Amini, M., Weis, D., 2015. A practical guide for the design and implementation of the double-spike technique for precise determination of molybdenum isotope compositions of environmental samples. Anal. Bioanal. Chem. 407, 1925–1935. http://dx.doi.org/10.1007/s00216-014-8448-6.
Skierszkan, E.K., Mayer, K.U., Weis, D., Beckie, R.D., 2016. Molybdenum and zinc stable isotope variation in mining waste rock drainage and waste rock at the Antamina mine. Peru. Sci. Total Environ. 550, 103–113. http://dx.doi.org/10.1016/j.scitotenv.2016.01.053.
Smedley, P.L., Kinniburgh, D.G., 2017. Molybdenum in natural waters: a review of occurrence, distributions and controls. Appl. Geochem. http://dx.doi.org/10.1016/j.apgeochem.2017.05.008. (in press), corrected proof.
Theobald, P.K., Lakin, H.W., Hawkins, D.B., 1963. The precipitation of aluminum, iron and manganese at the junction of deer creek with the snake river in summit county, Colorado. Geochim. Cosmochim. Acta 27, 121–132.
Tossell, J.A., 2005. Calculating the partitioning of the isotopes of Mo between oxidic and sulfidic species in aqueous solution. Geochim. Cosmochim. Acta 69, 2981–2993. http://dx.doi.org/10.1016/j.gca.2005.01.016.
USGS, 2005. Open-file Report 2005-1305 Preliminary Integrated Geologic Map Databases for the United States Western States: California. Nevada, Arizona, Washington, Oregon, Idaho, and Utah, Version 1.3, Updated December 2007.
Voegelin, A.R., Nägler, T.F., Pettke, T., Neubert, N., Steinmann, M., Pourret, O., Villa, I.M., 2012. The impact of igneous bedrock weathering on the Mo isotopic composition of stream waters: natural samples and laboratory experiments. Geochim. Cosmochim. Acta 86, 150–165. http://dx.doi.org/10.1016/j.gca.2012.02.029.
Voegelin, A.R., Pettke, T., Greber, N.D., von Niederhäusern, B., Nägler, T.F., 2014. Magma differentiation fractionates Mo isotope ratios: evidence from the kos plateau tuff (aegean arc). Lithos 190–191, 440–448. http://dx.doi.org/10.1016/j.lithos.2013.12.016.
Vorlicek, T.P., Kahn, M.D., Kasuya, Y., Helz, G.R., 2004. Capture of molybdenum in pyrite-forming sediments: role of ligand-induced reduction by polysulfides. Geochim. Cosmochim. Acta 68, 547–556. http://dx.doi.org/10.1016/S0016-7037(00)00444-7.
Wang, Z., Ma, J., Li, J., Wei, G., Chen, X., Deng, W., Xie, L., Lu, W., Zou, L., 2015. Chemical weathering controls on variations in the molybdenum isotopic composition of river water: evidence from large rivers in China. Chem. Geol. 410, 201–212. http://dx.doi.org/10.1016/j.chemgeo.2015.06.022.
Wasylenki, L.E., Rolfe, B.A., Weeks, C.L., Spiro, T.G., Anbar, A.D., 2008. Experimental investigation of the effects of temperature and ionic strength on Mo isotope fractionation during adsorption to manganese oxides. Geochim. Cosmochim. Acta 72,

5997–6005. http://dx.doi.org/10.1016/j.gca.2008.08.027.
Wiederhold, J.G., Teutsch, N., Kraemer, S.M., Halliday, A.N., Kretzschmar, R., 2007. Iron isotope fractionation during pedogenesis in redoximorphic soils. Soil Sci. Soc. Am. J. 71, 1840. http://dx.doi.org/10.2136/sssaj2006.0379.
Wilson, S.A., 1997. The collection, preparation, and testing of USGS reference material BCR-2, Columbia River, Basalt. U.S. Geological Survey Open-File Report 98-xxx. .
World Health Organization, 2011. Guidelines for Drinking-water Quality, fourth ed. http://dx.doi.org/10.1016/S1462-0758(00)00006-6.
Xu, N., Christodoulatos, C., Braida, W., 2006. Adsorption of molybdate and tetrathiomolybdate onto pyrite and goethite: effect of pH and competitive anions. Chemosphere 62, 1726–1735. http://dx.doi.org/10.1016/j.chemosphere.2005.06.025.